RSC Advances

PAPER

View Article Online
View Journal | View Issue

Cite this: *RSC Adv.*, 2022, **12**, 2759

2D graphene/FeOCl heterojunctions with enhanced tribology performance as a lubricant additive for liquid paraffin†

Mengxin Xie,[a] Bingli Pan,*[ab] Ning Li,[a] Shuang Zhao,*[a] Junjiang Yan,[a] Shihao Guo,[a] Zhe Chen[a] and Honggang Wang*[c]

The purpose of this study is to prepare graphene/FeOCl (G/FeOCl) heterojunctions *via* a microwave-pyrolysis approach and probe into the synergistic lubrication of G with FeOCl in liquid paraffin (LP). The morphology and chemical composition of specimens were analysed by utilizing scanning electron microscopy (SEM) with energy dispersive spectroscopy (EDS), X-ray diffraction (XRD), Fourier transform infrared (FTIR) spectroscopy, and X-ray photoelectron spectroscopy (XPS) techniques. The tribological property of G/FeOCl was determined, and the interaction between the G/FeOCl heterojunction and friction pair was carried out through simulation calculations. The results indicated that neither G nor FeOCl significantly improved the lubrication performance of LP. However, together with FeOCl, G as lubrication additives greatly improved the lubrication performance of LP. Under the load of 1.648 GPa, the mean friction coefficient and wear scar diameter of LP containing 0.20 wt% G/FeOCl were 66.1% and 44.7% inferior to those of pure LP, respectively. Scanning electron microscopy (SEM) and elemental mapping analyses of worn scars revealed the formation of G/FeOCl layer tribofilms that prevent direct contact between metals. In addition, the high interfacial energy between graphene and FeOCl calculated based on first-principles density functional theory (DFT) further confirmed that graphene and FeOCl simultaneously form friction films with wear resistance and wear reduction effect at the friction interface, which is consistent with the experimental results. This study, therefore, provides a pathway for low-friction lubricants by deploying G/FeOCl two-dimensional material systems.

Received 4th September 2021
Accepted 22nd November 2021

DOI: 10.1039/d1ra06650a

rsc.li/rsc-advances

1. Introduction

About 20% of the total energy production in the world is used to overcome friction. As mobility continues to increase, these numbers will no doubt skyrocket, posing huge challenges for sustainable transport.[1–3] Therefore, reducing friction and wear can not only improve the service life of machinery but also improve the energy efficiency. Lubricants are thought to reduce friction and wear by forming a stable lubricating film between the surfaces of the friction pairs. However, the potential of lubricant depends on factors such as additive concentration, composition, and molecular structure.[4] Among them, the molecular structure is particularly significant.

Recent trends in nanoscale additives and their derivatives have led to a proliferation of studies on two-dimensional nanomaterials with improved anti-wear and anti-friction behaviours.[5] With excellent mechanical properties, outstanding electrical and thermal conductivity, specific surface area, remarkable self-lubricating properties and superior thermal conductivity, graphene offers unique and interesting possibilities for structural and mechanical applications, making it stand out among 2D lubricating materials.[6,7] Furthermore, the weak van der Waals interlaminar forces between adjacent layers of G and intrinsically low adhesion enable easy lamellar shear and make it to prevent wear between contact surfaces in the process of mutual motion.[8,9] The ability of G to inhibit wear is due in part to its mechanical strength; Young's modulus of the order 1 TPa is equivalent to the in-plane elastic stiffness of G.[10,11] Inspired by these superiorities, sizeable efforts have been put into excavating graphene-based composites as nanoadditives to boost the antifriction and antiwear properties of base oils.[12] For instance, Tan *et al.* found that nanoporous graphite can significantly improve the wear resistance of phenolic resin.[13] Zhao *et al.* adopted the exfoliation method to inquire into the effect of different layer numbers and

[a]*Institute of Henan Polymer Composites, School of Chemical Engineering, Henan University of Science and Technology, 471000 Luoyang, PR China. E-mail: blpan@haust.edu.cn*

[b]*National United Engineering Laboratory for Advanced Bearing Tribology, Henan University of Science and Technology, 471000 Luoyang, PR China*

[c]*State Key Laboratory of Solid Lubrication, Lanzhou Institute of Chemical Physics, Chinese Academy of Sciences, Lanzhou, 730000, PR China*

† Electronic supplementary information (ESI) available. See DOI: 10.1039/d1ra06650a

layer spacing on the performance of graphene as lubrication additive and drew a conclusion that the degree of exfoliation is pivotal in the structural evolution of graphene, that is, highly exfoliated graphene indeed reaching interlayer slip, which can achieve superior lubrication.[14] Han *et al.* reported that imidazolyl dinitrile salt modified graphene improved the tribological and wear properties of PEG200, and the lubrication effect was derived from the protective layer formed on the friction pair interface by the modified graphene.[15] However, there are fewer functional groups on the surface of G, so the adhesion ability on the surface of the friction pair is weak. In addition, there are some challenges in improving the service life and carrying capacity of G. Heterostructures assembled from different two-dimensional materials obviously provide us with more possibilities to adjust the interface conditions and obtain specific properties we need.

Zhang *et al.* demonstrated that RGO/Fe_3O_4 could significantly improve the tribological properties of PAO6 due to the synergistic effect of RGO and Fe_3O_4.[16] Li *et al.* confirmed that graphene–Fe_3O_4 could enhance the binding between resin and fiber and improve its tribological properties.[17] Therefore, compounds containing iron are considered to have good friction lubrication potential. Iron oxychloride (FeOCl) is a self-stacking layer of oxygen halide formed by van der Waals forces. FeOCl as a functional material has attracted more and more attention for the past few years. Furthermore, the specific layer structure of FeOCl can promote electron transfer.[18] As is known, all compounds with layered structures are brilliant adsorption materials.[19] Nonetheless, FeOCl has a low band gap energy (about 1.8 eV), resulting in rapid carrier recombination. It has been reported that a possible way to improve the environmental stability of FeOCl is to structure a heterogeneous system with other materials.[20] Unfortunately, to the best of our knowledge, there have been no reports on the tribological properties of FeOCl.

Consequently, this study attempted to introduce G as a substrate to afford abundant attachment sites for FeOCl. On the basis of giving full play to the prominent adsorption properties of G and FeOCl, it is hoped that the incommensurate combination of G and FeOCl can further enhance the frictional properties. In this paper, a two-step simple microwave-pyrolysis approach for the synthesis of G/FeOCl heterojunctions was presented. Samples characterization results based on a scanning electron microscope (SEM) with EDS, X-ray diffractometer (XRD), Fourier transform infrared (FTIR), and X-ray photoelectron spectroscopy (XPS) analyses confirmed the successful synthesis of G/FeOCl heterojunctions. The tribo-performance of G/FeOCl heterojunctions as an additive to LP was probed using the four-ball friction machine. Field emission scanning electron microscopy (FESEM), and elemental mapping analysis were used to analyze the worn scars on the surface of the steel ball to understand the lubrication mechanism and action of friction and wear of G/FeOCl in LP. Furthermore, the interfacial energy between G and FeOCl was calculated *via* DFT, and the simulation results verified the conjectured mechanism of the experiment.

2. Materials and methods

2.1 Materials

Citric acid ($C_6H_8O_7 \cdot H_2O$, ≥99.5%, Tianjin Fengchuan Chemical Reagent Technologies Co., Ltd.), iron trichloride ($FeCl_3 \cdot 6H_2O$, ≥99.0%, Damao Chemical Reagent Factory), octadecylamine ($C_{18}H_{39}N$, ≥90.0%, Shanghai Jingchun Reagent Co., Ltd.) and *N*,*N*′-dicyclohexylcarbodiimide ($C_{13}H_{22}N_2$, ≥90.0%, Shanghai Macklin, Biochemical Co., Ltd.) were used as received without further purification. Acetone (CH_3COCH_3, ≥99.5%, Luoyang Haohua Chemical Reagent Co., Ltd.), liquid paraffin received from Tianjin Deen Chemical Reagent Corporation Limited, was used as lube base oil. All chemical reagents were used directly without further purification.

2.2 Preparation of G/FeOCl heterojunction

Graphene was synthesized by pyrolysis of citric acid in the light of the literature method.[21] A microwave-pyrolysis approach was applied to the preparation of G/FeOCl composites. In the first step, the crucible containing $FeCl_3 \cdot 6H_2O$ was sealed and kept in a microwave oven at low heat for 10 minutes. Afterward, the resulting reddish-brown FeOCl was slowly cooled to room temperature and ground into a powder. Due to the high solubility of ferric chloride in acetone, the product was cleaned with acetone to remove unreacted ferric chloride and to prevent the formation of ferric divalent. In the second step, FeOCl was mixed with citric acid at the mass ratio of 1 : 10 in a beaker under grinding evenly. Subsequently, the beaker containing the powder was sealed with polyimide tape, in which holes were punched, and carefully placed in an oven at 180 °C for pyrolysis for 30 minutes. After completion of pyrolysis, the acquisition was ground again after taking out and was separated by centrifugation. The product was repeatedly washed with acetone to remove the unspent reaction precursor and dried under vacuum at 80 °C.[22] Finally, the dark grey colored G/FeOCl heterojunction, was obtained.

2.3 Material characterizations

The phase structure of the as-prepared product was identified using a Bruker D8 advance X-ray diffractometer (XRD, range, 5–80°; scan rate, 5° min^{-1}). FTIR spectra of graphene-based samples were measured using Fourier transform infrared spectrometry (IRTracer-100) for detecting the chemical structure of powder samples. X-ray photoelectron spectroscopy (XPS) was conducted on PerkinElmer PHI-5300 ESCA to identify the chemical states and coordination environment of Fe in the product. The morphologies and images of the samples were captured using a scanning electron microscope (SEM). Energy-dispersive X-ray spectrometry (EDS) was used for qualitative chemical analyses.

2.4 Computational methods

First-principles calculations were performed using the DFT method, which enabled structural optimization of G/FeOCl model and computations of energy, as implemented in the

Dmol^3 code inlaid in the Material Studio software (Accelrys, SanDiego, CA).[23] Particularly, the exchange–correlation functional was depicted by the Generalized Gradient Approximation (GGA) of the Perdew–Burke–Ernzerhof (PBE), and a double numerical plus polarisation (DNP) basis set.[24] DFT Semi-core pseudopots (DSPP) was employed in core electronic treatment.[25,26] A 2 × 2 × 2 Monkhorst–Pack mesh was selected for sampling *k*-points in Brillouin region. Parameter settings in the simulation are shown in Table 1. The calculated energies were coordinated by a dispersion correction on the basis of the Tkatchenko and Scheffler methods (*i.e.*, a van der Waals DFT-D functional).[27] Furthermore, graphene was framed based on the $C_{48}H_{18}$ clusters (Fig. S1†), which was a simplified model to bring down the difficulty and complexity of calculation. The model of FeOCl was constructed based on the research of predecessors.[28] The value of the adsorption energy (E_{ads}) was calculated *via* the following formula:

$$E_{ads} = E_{G+FeOCl} - E_G - E_{FeOCl} \quad (1)$$

In the above formula, E_G, E_{FeOCl} and $E_{G+FeOCl}$ represent the energy of the graphene, the energy of the FeOCl molecule and the total energy of FeOCl adsorbed on the graphene surface, respectively. Negative adsorption energy is advantageous in energy.

2.5 Tribo-performance evaluation

An MM-W1 four-ball vertical universal friction test system controlled by a microcomputer (Jinan Puye Electromechanical Technology Co., Ltd, Jinan, China) was used to probe the tribological properties of prepared samples as a lubricating additive to liquid paraffin oils as per GB3142-82 and ASTM5183-95 standards. The friction and wear tests were carried out under 1.648 GPa and 1000 rpm for 30 min test duration. Steel balls, which are composed of GCr15 bearing steel (hardness: 61–66 Hardness Rockwell C (HRC), and diameter: 12.7 mm) were used in this work. Pre- and post-cleaning of the balls was performed using acetone by ultra-sonication followed by drying. Three replicate friction and wear tests were conducted under a preset condition so as to minimize data scattering. At the end of each test, the wear scar diameter (WSD) of each of the three lower stationary balls was measured by the image acquisition system (±0.01 mm) of the four-ball tester. The average WSD of three lower balls was calculated and reported in this paper. After the wear test, the morphologies of the worn surfaces were detected using SEM, and chemical compositions of the wear scar surfaces were analyzed by elemental mapping.

3. Results and discussion

3.1 Structural and morphological features of lubricant additive

SEM images of FeOCl, G, and G/FeOCl heterojunction are displayed in Fig. 1a–c, respectively. From the magnified SEM image (Fig. 1a), it can be seen that FeOCl was composed of a great many ruleless plates, and the interlayer interface was not visible.[22] Fig. 1c perspicuously revealed FeOCl garnishing G sheet, and the size of the binary hybrid was obviously smaller than that of a single component, presenting a lamellar structure with stacked nanosheets.[29] The chemical composition of G/FeOCl was obtained from its mapping and EDS spectrum (Fig. 1d). Signals due to carbon, oxygen, and ferrum along with chlorine were clearly visible in the spectrum, indicating the formation of the proposed heterojunction. The embedded atom distribution and atomic weight% data in Fig. 1d reflected the formation of the G/FeOCl heterojunction.

The XRD patterns of the synthesized FeOCl and G/FeOCl are shown in Fig. 2a. The obvious characteristic diffraction peaks of FeOCl and G/FeOCl were located at 11.43, 26.41, 35.78 and 38.23 corresponding to (010), (110), (021), and (111) crystal facets, respectively. These findings can be assigned to the pure phase of FeOCl as per orthorhombic lattice, JCPDS no. 24-1005 and JCPDS no. 72-0619.[30] The (010), (110), and (021) peak intensities of G/FeOCl were significantly weaker than that in FeOCl, which was caused by the effect of G embedded in the FeOCl lattice on both sides of the crystallites, thus reducing the size of G/FeOCl, which was consistent with the results of SEM measurements.

FT-IR spectrum was used to reveal the successful synthesis of the G/FeOCl hybrid. The FTIR spectrum (Fig. 2b) of G/FeOCl displays the presence of C=O (1716 cm^{-1}), C=C (1610 cm^{-1}), –COOH (1269 cm^{-1}) and Fe–O (636 cm^{-1}).[29,31] The typical functional groups of GO can be seen in the FT-IR of heterojunctions, indicating the successful composite of G and FeOCl.

In order to verify the chemical structure of G/FeOCl heterozygote, XPS measurements were used to investigate both FeOCl and G/FeOCl. The full-range XPS spectrum of the heterozygote (Fig. 3e) clearly shows the photoelectron peak signals of Fe, Cl, O and C, with atomic% of 5.79, 2.04, 30.77, and 61.40, respectively, which further verifies that G and FeOCl coexist in the heterojunction. The core-level spectrum after optimal fitting parameter deconvolution based on Thermo Avantage software is shown in Fig. 3. Fig. 3a clearly exhibits core-level spectra of C 1s deconvoluted into four peaks with binding energies of 284.6, 285.7, 287.8, and 288.9 eV corresponding to C–C, C–O, C=O, and O–C=O bonds, respectively.[32] Fig. 3b shows the O 1s spectrum of G/FeOCl composite material. The oxygen in G/FeOCl material was mainly decomposed into two peaks,

Table 1 Parameters used in the simulation

Parameter	Self-consistent field[a] (Ha per atom)	Energy[a] (Ha per atom)	Maximum force[a] (Ha Å^{-1})	Maximum displacement[a] (Å)	Smearing value[b]
Value	1.0×10^{-6}	1.0×10^{-5}	2.0×10^{-3}	5.0×10^{-3}	5.0×10^{-3}

[a] Parameters applied to optimize the structure. [b] Represents the parameter used for track occupancy.

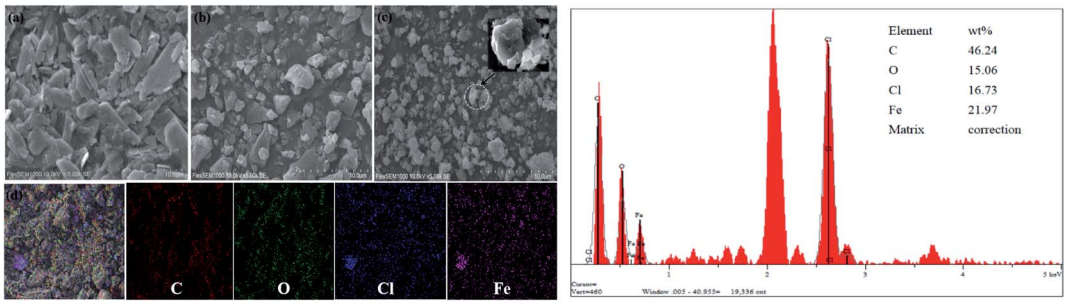

Fig. 1 SEM images of (a) FeOCl, (b) G, (c) G/FeOCl and (d) the mapping and the EDS spectrum of G/FeOCl.

which were similar to the peaks of FeOCl in Fig. S1c.† The peak at 530.8 eV matched Fe–O in the FeOCl lattice while the peak at 532.6 eV was attributed to adsorbed oxygen on the surface.[33,34] Fig. 3c shows core-level spectra of Cl 2p deconvoluted into two distinct peaks at 197.1 eV and 198.8 eV, which belong to Cl 2p of Cl in G/FeOCl heterozygote.[35] Compared with the Cl 2p peak of FeOCl (Fig. S1a†), the Cl 2p peak of G/FeOCl moved to a higher level, which was the result of the interaction between G and Cl.[29] The peaks of Fe 2p in FeOCl (Fig. S1b†) were centered at 711.7 eV and 725.5 eV, corresponding to the spin–orbit peaks of Fe $2p_{3/2}$ and Fe $2p_{1/2}$, respectively, indicating that Fe element appears in the Fe(III) state.[36] The Fe 2p peaks (710.4 eV and 723.8 eV) of G/FeOCl shifted towards a lower direction than that of FeOCl (Fig. 3d), which was the result of the interaction between FeOCl and G.[29,37] The XPS spectra of G/FeOCl further confirmed the successful heterozygosity of FeOCl and G.

3.2 Assessment of tribological behaviour of lubricant additives in LP

3.2.1. Dispersion stability. The dispersion stabilities of the G/FeOCl heterojunction in LP were studied by the absorbance method. Primarily, as-prepared samples were ultrasonically dispersed in LP for 1 h. After the friction test, it was found that the optimal concentration of the sample in the base oil is 0.20 wt%. The absorbance of a solution that had been diluted by 10 times was elucidated at different time intervals by a visible-721 spectrophotometer. The absorbance of different dispersions was monitored at different time intervals from 0 to 48 h at a wavelength of 350 nm.[3,38] Fig. 4a displays the dispersion of the proposed G, FeOCl and G/FeOCl lubricant samples at 0.20 wt% in LP. Fig. 4b shows a graph of the relative absorbance of each additive as a function of precipitation time. The higher the peak absorbance of the lubricant additive was, the better was its dispersion in the base oil.[39] The results of the visible spectrum showed that G/FeOCl had good stability within 2 d after mixing. It is worth noting that the stability of the lubricant decreased with the increase of storage time due to the deposition of lubricating additives into the base oil. According to Derjaguin, Landau, Verwey, and Overbeek (DLVO theory), when the repulsive force between materials was lower than the Brownian motion and van der Waals attraction of materials, additives will undergo agglomeration.[40] In this study, the dispersions were again subjected to ultrasound for 1 h before the tribology experiment to reduce aggregation and deposition of particles in LP. Therefore, the factors affecting dispersion stability need to be further studied.

3.2.2. Friction reduction. For the assessment of anti-wear properties, four-balls MM-W1A tests of liquid paraffin with its admixtures were conducted. The optimum concentration for the application was 0.20 wt% at 1.648 GPa load and 1000 rpm for 15 min test duration. Fig. 5b presents the friction coefficient for LP with different additives. It can be seen that with the increase of sliding time, the LP mixed with these lubricant additives had a lower friction coefficient and was more stable than the pure LP. Fig. 5a summarizes the mean coefficient of

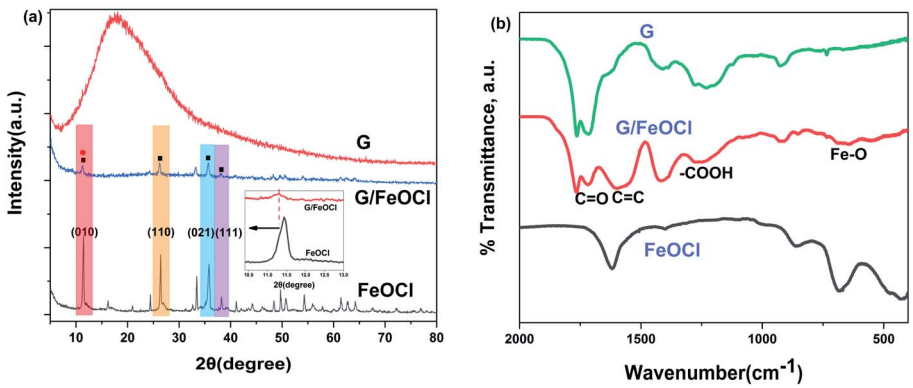

Fig. 2 (a) XRD pattern; (b) FT-IR spectra of G, FeOCl and G/FeOCl.

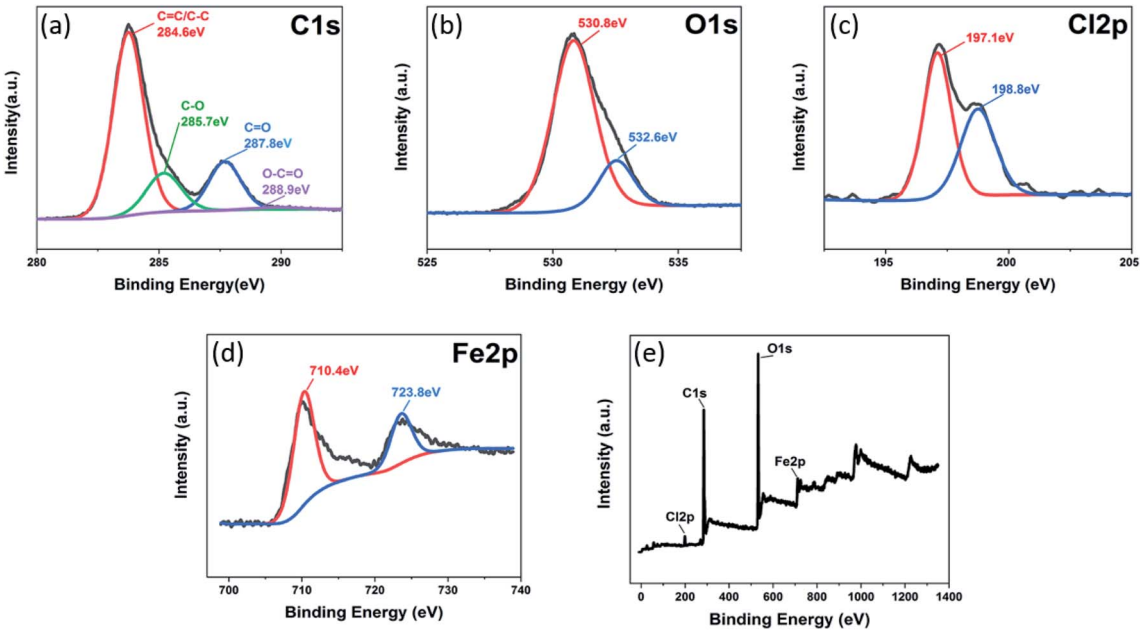

Fig. 3 XPS images of G/FeOCl heterozygote: (a) C 1s core-level spectra, (b) O 1s core-level spectra, (c) Cl 2p core-level spectra, (d) Fe 2p core-level spectra, and (e) XPS survey spectra.

friction (MCOF) in the absence and presence of different additives in LP. Obviously, LP with 0.20 wt% G/FeOCl additive exhibited the optimal friction performance, possessing the lowest and most stable friction coefficient during running time. The MCOF for steel tribopairs using LP lube oil was estimated to be 0.078 with a broad range of standard deviations. All samples as LP additives significantly reduced the COF. There was a slight improvement in the anti-friction properties of the LP in the presence of individual G or FeOCl, which reduced the COF by 16.2% and 34.3%, respectively. It is noteworthy that the MCOF of LP containing G/FeOCl heterozygote these values increased further to a greater degree. The 0.20 wt% of G/FeOCl exhibited the lowest MCOF, 66.1% lower than LP lube oil, which indicated the vital function of G/FeOCl in the running process. In conclusion, G/FeOCl particles can improve the anti-friction performance of LP, and its anti-friction effect was better than that of G and FeOCl.[41] The results were verified by using typical trend charts of different oil sample friction coefficients, as shown in Fig. 5b.

Subsequently, the tribology performance of LP with different concentrations of G/FeOCl heterozygote (from 0.00 wt% to 2.00 wt%) was performed (Fig. 5c). The MCOF decreased with the dose of G/FeOCl increased from 0.00 wt% to 0.20 wt% in LP, it was obviously observed that the COF decreased gradually from 0.078 to 0.027, which was the lowest among all the concentrations. Subsequently, as the concentration of G/FeOCl heterozygote increased from 0.20 wt% to 2.00 wt%, the COF value of LP increased finally reaching 0.049. These results explicitly suggested that with the change in the G/FeOCl heterozygote addition concentration in LP, the optimal concentration was 0.20 wt% for the antifriction performance, and the corresponding MCOF decreased to 0.027. This may be

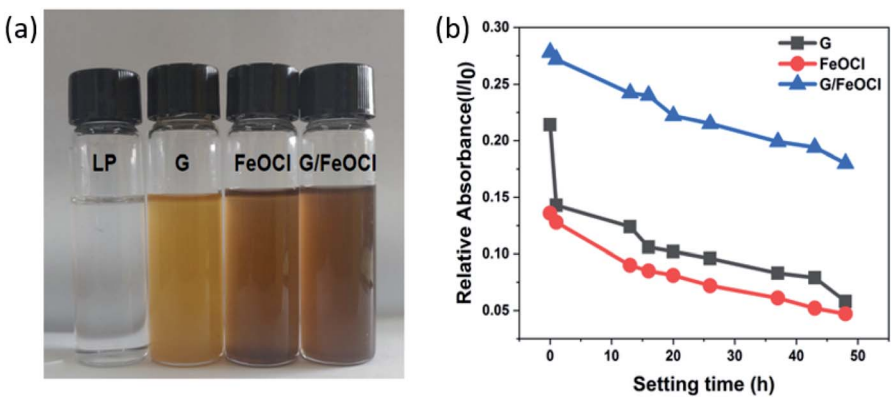

Fig. 4 (a) Lubricant samples and (b) dispersion stabilities of base oil containing G, FeOCl, and G/FeOCl studied by UV-vis spectrophotometry.

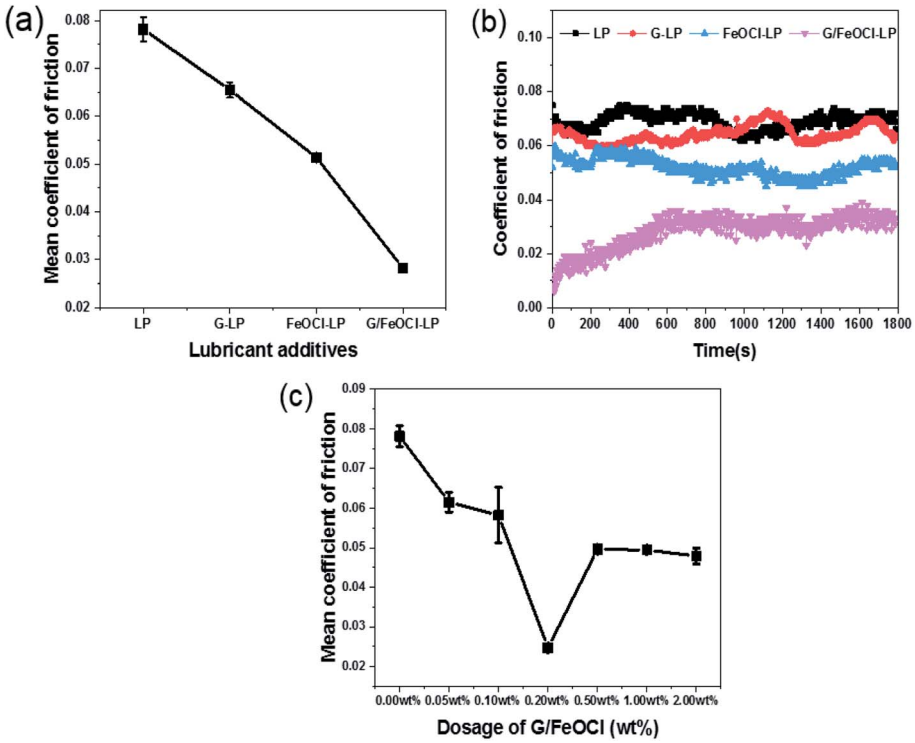

Fig. 5 (a) Comparison of mean friction coefficient of LP containing different samples (0.20 wt%) under certain conditions; (b) friction coefficients for all samples as a function of run time; (c) mean coefficient of friction using (1.648 GPa, 1000 rpm, 30 min).

due to the saturation of the contact area between the friction pairs with lubricating additives when the boundary lubrication state was dominant.[38] In the case of friction coefficient analysis of graphene lubrication additives, the COF reported by Varrla *et al.* decreased from 0.10 to (base oil) to 0.02 (0.02 wt% graphene).[42] The friction coefficient of graphene-based composites studied by Yang *et al.* decreased from 0.104 of pure paraffin oil to 0.08 (including 0.50 wt% graphene-based composites).[31] In this case, a concentration of 0.20 wt% can help the additive fill the valley in the concave–convex body, thereby reducing COF.

The significant decrease in MCOF value after the addition of the above additives was directly related to their antifriction performance. This behaviour can be explained by the key role that different additives play in the formation of tribochemical films (*in situ*), which prevented proximal surface contact and was essential for reducing friction on the proximal surface.[3] However, the presence of oxygen-containing functional groups, structural ripples, and high shear resistance due to hydrogen bonding between adjacent atomic layers in G had a negative impact on the tribological properties.[43] Thus, the obtained results indicated that CM G/FeOCl had better lubrication performance than G, FeOCl and PM G/FeOCl, which may be due to the synergistic lubricating role of G and FeOCl. The difference in lubrication performance between PM G/FeOCl and CM G/FeOCl heterozygote indicates that the synergistic lubrication effect of G and FeOCl had a close relationship with the microstructure of the heterozygote.[44] These atoms or molecules interacted with each other under frictional stress conditions and/or interact with the surface of the interacting steel balls to form a protective film between the friction pairs to prevent direct contact between steel balls.[45] An overview of typical graphene composites used as lubricant additives are displayed in Table 2.

3.2.3. Wear resistance. The wear resistance of G, FeOCl, and G/FeOCl in LP under 1.648 GPa for 15 min test duration was measured by a four-ball testing machine. The test results are presented as a bar graph in Fig. 8, which simulates a comparison graph of mean wear scar diameter (MWSD). Fig. 6a summarizes the MWSD in the absence and presence of different additives in LP. Obviously, the LP with 0.20 wt% G/FeOCl additive exhibited the optimal friction performance, showing the lowest and most stable friction coefficient during running time. The MWSD for steel tribopairs using LP lube oil was estimated to be 0.80 mm with a broad range of standard deviation. All samples as LP additives significantly reduced MWSD. The anti-wear properties were also improved to a certain extent in presence of individual G or FeOCl, in which the MWSD decreased slightly. That is, the use of individual G or FeOCl in LP could prevent severe wear on the surface of steel balls during the running process.[46] It is noteworthy that the 0.20 wt% of G/FeOCl exhibited the lowest MWSD, 44.7% lower than LP lube oil, which indicates the vital function of G/FeOCl in the running process. The significant decrease in MWSD value after the addition of the above additives was directly related to their wear resistance and antifriction performance. The increase in load results in greater pressure on the contact surface, which reduced the film thickness and promotes contact with the

Table 2 Graphene composites as lubricant additives

Lubricant details				Conditions			Tribological test results		
Materials	Concentration	Base oil	Tribometer	Load	Speed	Temperature	Wear reduction, %	Friction reduction, %	Ref.
Hydroxyl modified fluorinated graphene	1 mg mL^{-1}	Water	Ball-on-disk tribometer	50 N	0.05 m s^{-1}	25 °C	—	15%	47
Graphene	0.025 mg mL^{-1}	Engine oil	Four-ball	392 N	600 rpm	75 °C	33%	80%	42
GO/f-CMS	0.2 wt%	85W-90	BOD	40 N	—	—	54%	26%	48
Cu/Gr	0.4 wt%	5W-30	Ring-liner	216–307 N	0.25 m s^{-1}	—	25–30%	26.5–32.6%	39
Titanate-GO	0.3 mg mL^{-1}	PAO10	Four-ball	392 N	1200 rpm	75 °C	28.2%	49.5%	49
OA–LaF_3–GO	0.5 wt%	Liquid paraffin	Four-ball	300 N	1450 rpm	25 °C	32%	21.7%	50
RGO/MoS_2	0.02–0.08 wt%	Liquid paraffin	Ball-on-disk	50 N	0.04–0.05 m s^{-1}	—	—	45%	51

bulges on the ball surface, thereby increasing the MWSD measurement.

Fig. 6b depicts the change curve of MWSD at different concentrations of G/FeOCl at a load of 1.648 GPa for 15 min in base lube LP. It is clear from Fig. 7b that MWSD values of LP with all concentrations additives were significantly reduced compared to the pure LP. Therefore, G/FeOCl heterojunctions were capable of promoting the wear resistance of LP at each concentration. Fig. 7 portrays digital images of WSD at different G/FeOCl hybrid concentrations. These digital pictures were taken from one of the measurements of the diameter of the wear scar. It can be seen clearly that the WSD of LP containing 0.20 wt% G/FeOCl was the minimum, further demonstrating that its optimal concentration was 0.20 wt%. The LP with 0.20 wt% G/FeOCl exhibited the lowest MWSD (0.44 mm), 44.7% lower than that of pure LP. A further increase dosage of G/FeOCl showed no significant change in the wear resistance. When the concentration of additive was exorbitant, particles tended to agglomerate under the friction-induced effect. The existence of large particles can preclude the small size of G/FeOCl heterojunction from entering the friction zone. Additionally, once large particles are turned into the friction area, it is highly likely that abrasive particles will be formed, increasing friction and thus accelerating surface wear.[52] Considering the antifriction and antiwear comprehensively, the optimal concentration of G/FeOCl in LP was 0.20 wt%. The variation trend of the MWSD under different loads and rotating speeds was consistent with the friction coefficient. Under operating conditions, the stable heterostructures were easily transferred and deposited into the contact zone on the surface of the friction pair, forming *in situ* a tribochemical film with low shear strength, which can resist direct metal-to-metal contact and protect it from friction and wear.[53] In fact, G and FeOCl, both of which have layered structures, worked together to improve the efficiency of the composites. The performance of the composites was superior to that of single-component G or FeOCl, which can be explained by the fact that the thermal conductivity of the G/FeOCl hybrid was higher than that of the single component, thereby reducing the local temperature at the metal surface roughness.[31] Therefore, heat dissipation provides higher tribological properties.

3.2.4. Morphological studies of worn surface. The wear tracks on the steel ball surface lubricated with LP and its blends containing different additives (0.20 wt%) were analyzed by SEM

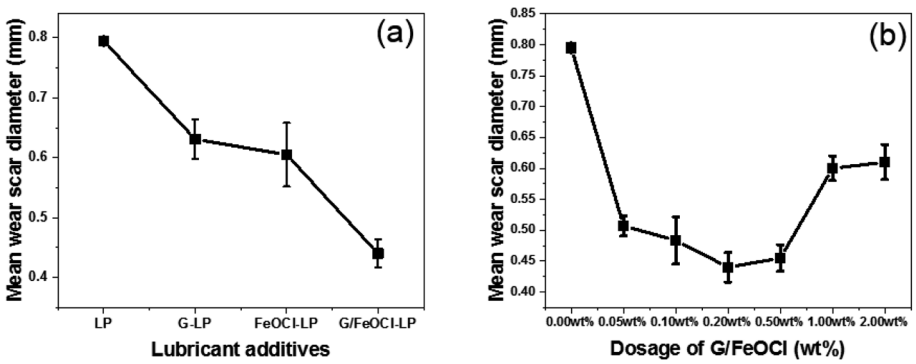

Fig. 6 Variation of mean wear scar diameter with (a) different additives; (b) different dosage of G/FeOCl (1.648 GPa, 1000 rpm, 15 min).

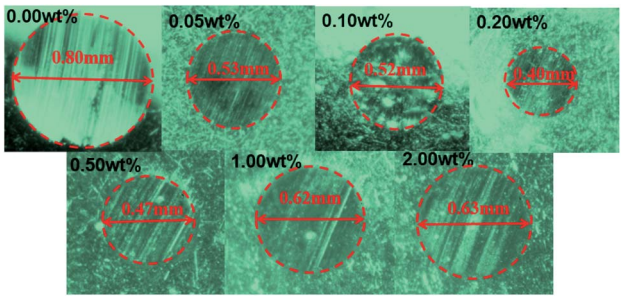

Fig. 7 Optical pictures of WSD at various G/FeOCl hybrids concentration.

and EDS measurements to understand the effect of G/FeOCl lubrication additives on reducing wear. As shown in Fig. 8, the wear surface of the steel ball with pure LP was very rough, with many wide and deep grooves in the center and edge areas of the wear mark. In the presence of LP, enormous abrasion diameters (0.80 mm) and a large number of tearing points in the wear area indicated that the plastic deformation of the steel surface caused severe adhesive wear and tremendous surface damage.[54] The wear marks on the surface of the ball were undoubtedly improved in the presence of all the additives. The dispersion of graphene largely subsidized the width of the wear tracks, and no measurable pitch features were found in the wear tracks. This may be due to the protective effect of the deposition of graphene-based protective film on the friction interface.[44] As can be seen from Fig. 8, after the friction test in LP containing FeOCl, the surface of the steel ball was seriously oxidized, which masked the original appearance of the steel ball. However, in the presence of FeOCl, the size of the wear mark decreased slightly compared with that of pure LP, indicating that FeOCl played a certain role in reducing wear. Furthermore, in the case of G/FeOCl filling the oil-lubricated wear surface, there were fewer and shallow grooves and wear grooves. Importantly, the G/FeOCl heterozygote as lubricating additive was better than the individual G or FeOCl to improve the anti-wear ability of the LP, which was clearly derived from the minimum MWSD (44.7%, 30.3%, and 27.3% lower than for pure paraffin, G, and FeOCl, respectively). As shown in Fig. 8, although there are a few grooves and pits on the worn surface of G/FeOCl, most parts are smooth, which has a good correlation with their observed tribological behaviour. This indicates that the formation of a high-quality friction-induced film of G/FeOCl hybrid, which protected the steel ball surface from severe wear.[43]

The elemental mapping of the tribofilm formed by the binary heterojunction (G/FeOCl) blended with LP at a loading of 1.648 GPa is shown in Fig. 9, providing information on its elemental composition. The presence of C, O, Fe and Cl elements on the worn steel surface indicates that a tribochemical reaction occurred during sliding. Namely, the G/FeOCl hybrid can easily get into the interface of the friction pair to fill the cracks on the friction surface and prevent direct contact between steel and steel. Simultaneously, the G/FeOCl hybrid was decomposed to form a reactive film to protect the surface of the steel, thus improving the anti-friction and anti-wear ability of LP.[44]

3.3 Friction and wear mechanism analysis

Fig. 10 displays the lubrication mechanism. In view of the above analytical data and discussion, the lubrication mechanism of the significantly improved tribological performance of the G/FeOCl-LP oil lubrication mixture can be interpreted by the interaction of the G/FeOCl heterojunction with the sliding surface. It is well known that the properties of the friction film play a dominant part in the entire efficiency of the additive. Under experimental test conditions with actual load-bearing, the roughness of the steel ball surface permitted G/FeOCl to enter and cling to the proximal surface, forming a friction film *in situ*, which can bear the load. However, the fabulously excellent performance of the designed binary G/FeOCl heterogeneous material highlighted the synergistic effect between its constituent FeOCl and G. During the lubrication process, FeOCl

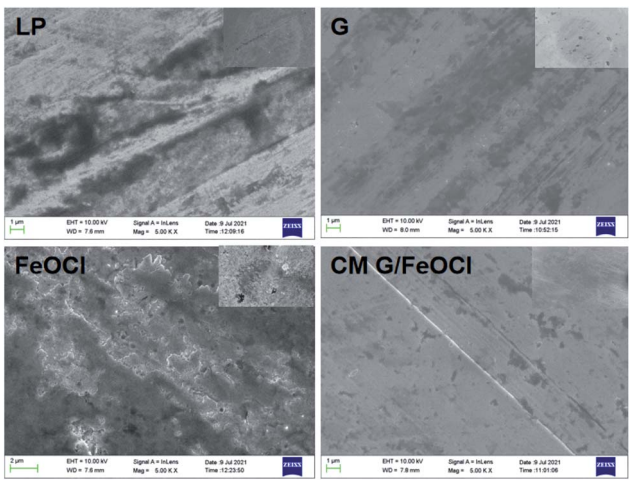

Fig. 8 SEM images (inset: full view of wear scar at 300×, wear scar surface at 5.00k× magnification) of the worn steel surface lubricated with LP in the presence and absence of different additives (0.20 wt%) for 15 min test duration at 1.648 GPa applied load.

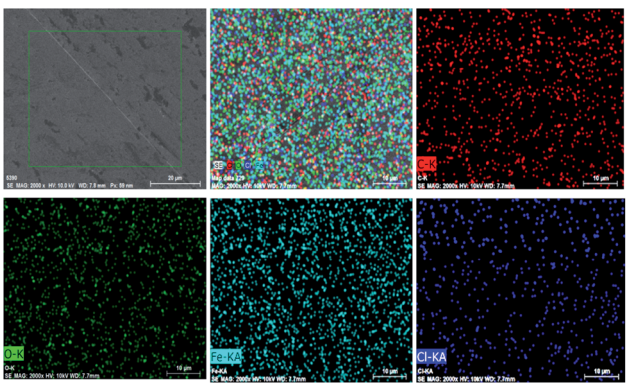

Fig. 9 EDS spectra of the worn steel surface lubricated with LP in the presence of G/FeOCl (0.20 wt%) for 15 min test duration at 1.648 GPa applied load.

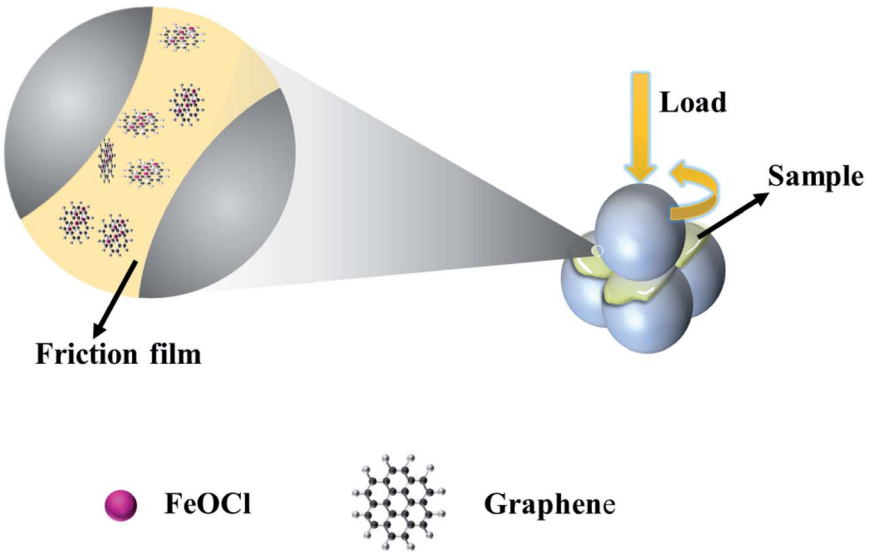

Fig. 10 Schematic diagram showing the lubrication mechanism of the heterojunctions of G and FeOCl.

and G complemented each other by sustaining their layered structure rather than crushing into small particles, and the heterojunction of the layered structure facilitated interlaminar sliding.[44] Over time, scratches and grooves, created on the interacting surfaces, were filled with G/FeOCl dispersions. The heat generated by the interface friction caused a tribological chemical reaction that contributes to the formation of a steady tribo-film between the interacting pairs. In order to further prove the friction film formed by FeOCl and G at the friction interface simultaneously, the interaction between graphene and FeOCl was investigated by the first-principles calculation on account of DFT. Fig. S2† portrays the optimized stable structure of graphene adsorption with FeOCl. The value of E_{ads} calculated using formula (1) was −3.64 eV. The negative value of the obtained binding energy indicates that FeOCl tended to adsorb graphene.[55] It manifested that physical adsorption existed between FeOCl and graphene. It is confirmed that the friction film was formed by FeOCl and G at the friction interface simultaneously. This friction film served on a third body, namely, the tribo-film formed a protective layer, which reduced the friction and wear on the interface.[56] The polishing effect of the studied heterojunction on the worn surface was also considered for improving the lubrication.[57] Based on the above mechanism, the prepared G/FeOCl heterojunctions have outstanding tribological properties.

4. Conclusions

The deployment of an intercalated composite 2D material system provides a way for graphene to be used as a low friction lubricant. This work has placed forward a newfangled synthesis approach, a fast and efficient microwave-pyrolysis method, to manufacture the G/FeOCl heterojunction with a layered structure, which was applied to a lubrication additive for tribological studies. G/FeOCl has been triumphantly synthesized and characterized using miscellaneous states of the art technologies as per powder XRD, FTIR, XPS, and SEM with EDS mapping. The tribological behaviours of G/FeOCl as the lubricant additives of LP were systematically investigated using a four-ball tribometer under a boundary lubrication regime. It is worth mentioning that the intercalation structure of G/FeOCl played a vital role in regulating its tribological behaviour. At an optimal dosage of 0.20 wt% for G/FeOCl, the average COF and MWSD of LP were reduced by up to 66.1% and 44.7%, respectively. In addition, G/FeOCl shows prominent bearing capacity, long service life and great operation stability, which reflects its huge potential for practical applications. Crucially, the synergistic lubrication effects of graphene and FeOCl were revealed by FE-SEM images, EDS elemental mappings and established as the elementary lubrication mechanism of G/FeOCl as lubricant additives of LP. This work not only provides a universal and feasible approach for preparing graphene-based composites with extraordinary lubricity but also elucidates the synergy of inorganic and organic materials on the boundary lubrication process.

Author contributions

Conceptualization, M. X. and B. P.; methodology, M. X., Z. C., and S. G.; software, N. L.; validation, M. X. and B. P.; formal analysis, M. X. and B. P.; investigation, M. X.; resources, B. P.; data curation, M. X.; writing—original draft preparation, M. X.; writing—review and editing, M. X.; visualization, J. Y.; supervision, B. P.; project administration, B. P.; funding acquisition, B. P. All authors have read and agreed to the published version of the manuscript.

Conflicts of interest

There are no conflicts to declare.

Acknowledgements

The authors sincerely thank the financial support from the National Natural Science Foundation of China (grant number 51675162) and the National SRTP (202110464023).

References

1 S. Kumari, A. Chouhan, O. P. Sharma, S. Kuriakose and O. P. Khatri, *ACS Appl. Mater. Interfaces*, 2020, **12**, 30720–30730.
2 A. Erdemir, G. Ramirez, O. L. Eryilmaz, B. Narayanan and S. Sankaranarayanan, *Nature*, 2016, **536**, 67–71.
3 D. K. Verma, N. Shukla, B. Kumar, A. K. Singh, K. Shahu, M. Yadav, K. Y. Rhee and R. B. Rastogi, *Nanomaterials*, 2020, **10**, 707.
4 M. Ratoi, V. B. Niste, H. Alghawel, Y. F. Suen and K. Nelson, *RSC Adv.*, 2013, **4**, 4278–4285.
5 S. Zhang, T. Ma, A. Erdemir and Q. Li, *Mater. Today*, 2019, **26**, 67–86.
6 B. Vasi, A. Matkovi, U. Ralevi, M. Beli and R. Gaji, *Carbon*, 2017, **120**, 137–144.
7 Y. Liu, X. Ge and J. Li, *Appl. Mater. Today*, 2020, **20**, 100662.
8 D. Berman, A. Erdemir and A. V. Sumant, *ACS Nano*, 2018, **12**, 2122–2137.
9 J. Zhao, B. Pan, Y. Zhang and Y. Zhang, *J. Macromol. Sci., Part B: Phys.*, 2012, **51**, 1218–1227.
10 G. H. Lee, R. C. Cooper, S. J. An, S. Lee, A. Zande, N. Petrone, A. G. Hammerberg, C. Lee, B. Crawford and W. Oliver, *Science*, 2013, **340**, 1073–1076.
11 M. R. Vazirisereshk, H. Ye, Z. Ye, A. Otero-De-La-Roza and A. Martini, *Nano Lett.*, 2019, **19**, 5496–5505.
12 D. Berman, S. A. Deshmukh, S. K. R. S. Sankaranarayanan, A. Erdemir and A. V. Sumant, *Science*, 2015, **348**, 1118–1122.
13 J. Tan, B. Pan, L. Hua, J. Chen, J. Liu, Y. Zhang and Q. Niu, *J. Macromol. Sci., Part B: Phys.*, 2019, 1–11.
14 J. Zhao, J. Mao, Y. Li, Y. He and J. Luo, *Appl. Surf. Sci.*, 2017, **434**, 21–27.
15 Z. Y. Han, C. L. Gan, X. P. Li, P. Feng, X. L. Ma, X. Q. Fan and M. H. Zhu, *Tribol. Int.*, 2021, **161**, 107057.
16 Q. Q. Zhang, B. Wu, R. H. Song, H. Song, J. Zhang and X. G. Hu, *Tribol. Int.*, 2020, **141**, 105952.
17 H. L. Li, L. Jin, J. L. Dong, L. Liu, M. Li, Y. Liu, L. H. Xiao and Y. H. Ao, *RSC Adv.*, 2016, **6**, 60200–60205.
18 M. Sun, I. Zucker, D. M. Davenport, X. Zhou, J. Qu and M. Elimelech, *Environ. Sci. Technol.*, 2018, **52**, 8674–8683.
19 L. Ai, Y. Zeng and J. Jiang, *Chem. Eng. J.*, 2014, **235**, 331–339.
20 J. Song, M. Zhang, C. Yan, X. Zhao and J. Zhang, *J. Alloys Compd.*, 2020, **836**, 155544.
21 Y. Dong, J. Shao, C. Chen, L. Hao, R. Wang, Y. Chi, X. Lin and G. Chen, *Carbon*, 2012, **50**, 4738–4743.
22 X. Liu, W. Zhang, L. Mao, Y. Yin and L. Hu, *J. Mater. Sci.*, 2021, **56**, 1–15.
23 B. Delley, *Lett. Nuovo Cimento*, 2000, **8**, 361–364.
24 J. P. Perdew, K. Burke and M. Ernzerhof, *Phys. Rev. Lett.*, 1998, **77**, 3865–3868.
25 M. Shukri, M. Saimin, M. K. Yaakob, M. Yahya and M. Taib, *Appl. Surf. Sci.*, 2019, **494**, 817–828.
26 S. S. Huang, B. L. Pan, M. X. Xie, J. Y. Gao, G. M. Zhao, Y. M. Niu and H. G. Wang, *Tribol. Int.*, 2020, **154**, 106726.
27 A. Tkatchenko and M. Scheffler, *Phys. Rev. Lett.*, 2009, **102**, 69–72.
28 X. J. Yang, P. F. Tian, X. M. Zhang, X. Yu, T. Wu, J. Xu and Y. F. Han, *AIChE J.*, 2015, **61**, 166–176.
29 J. Zhang, G. D. Liu and S. Liu, *New J. Chem.*, 2018, **42**, 6896–6902.
30 C. Tan, Q. Xu, T. Sheng, X. Cui and H. Li, *J. Hazard. Mater.*, 2020, **398**, 123084.
31 C. Yang, X. Hou, Z. Li, X. Li, L. Yu and Z. Zhang, *Appl. Surf. Sci.*, 2016, **388**, 497–502.
32 V. Jaiswal, K. Kalkhanday, S. Umrao, R. B. Rastogi, R. Kumar and A. Srivastava, *ACS Appl. Mater. Interfaces*, 2016, **8**, 11698–11710.
33 J. Zhao, M. Ji, J. Di, Y. Zhang and J. Xia, *J. Photochem. Photobiol., A*, 2019, **391**, 112343.
34 Y. Wang, H. Zhang, Y. Zhu, Z. Dai, H. Bao, Y. Wei and W. Cai, *Adv. Mater. Interfaces*, 2016, **3**, 1500801.
35 M. Sabri, A. Habibi-Yangjeh, H. Chang and V. Krishnan, *Sep. Purif. Technol.*, 2020, **250**, 117268.
36 C. Wan, J. Yue, W. Bao, G. He, Y. Wu and L. Jian, *J. Mater. Chem. A*, 2019, **7**, 9556–9564.
37 J. Zhang, M. Yang, Y. Lian, M. Zhong, J. Sha, G. Liu, X. Zhao and S. Liu, *Dalton Trans.*, 2019, **48**, 3476–3485.
38 S. Xiong, B. Zhang, S. Luo, H. Wu and Z. Zhang, *Friction*, 2020, 1–11.
39 M. K. A. Ali, X. Hou and M. A. A. Abdelkareem, *Friction*, 2020, **8**, 905–916.
40 M. Ali, H. Xianjun, L. Mai, C. Qingping, R. F. Turkson and C. Bicheng, *Tribol. Int.*, 2016, **103**, 540–554.
41 W. Song, P. Chen, J. Yan, W. Zhu and H. Ji, *ACS Appl. Mater. Interfaces*, 2020, **12**, 29737–29746.
42 V. Eswaraiah, V. Sankaranarayanan and S. Ramaprabhu, *ACS Appl. Mater. Interfaces*, 2011, **3**, 4221–4227.
43 A. Chouhan, S. Kumari, S. S. Rawat and O. Khatri, *ACS Appl. Mater. Interfaces*, 2020, **12**, 51785–51796.
44 Y. Xu, Y. Peng, K. D. Dearn, X. Zheng, L. Yao and X. Hu, *Wear*, 2015, **342**, 297–309.
45 V. Jaiswal, K. Kalkhanday, S. Umrao, R. B. Rastogi, R. Kumar and A. Srivastava, *ACS Appl. Mater. Interfaces*, 2016, 11698.
46 P. Wu, X. Chen, C. Zhang, J. Zhang and J. Zhang, *Friction*, 2020, **9**, 143–154.
47 L. M. Ma, Z. P. Li, W. H. Jia, K. M. Hou, J. Q. Wang and S. R. Yang, *Colloids Surf., A*, 2020, **610**, 125931.
48 Y. Gu, J. Fei, J. Huang, L. Zhang, M. Qu and X. Zheng, *Mater. Today Commun.*, 2020, **25**, 101271.
49 L. Zhang, X. Sun, X. Liu, Y. He, Y. Chen, Z. Liao, H. Gao and S. Wang, *ACS Omega*, 2021, **6**, 3840–3846.
50 C. Z. Yang, X. Hou, Z. W. Li, X. H. Li, L. G. Yu and Z. J. Zhang, *Appl. Surf. Sci.*, 2016, **388**, 497–502.
51 K. M. Hou, J. Q. Wang, Z. G. Yang, L. M. Ma, Z. F. Wang and S. R. Yang, *Carbon*, 2017, **115**, 83–94.
52 B. Jin, J. Zhao, G. Chen, Y. He and J. Luo, *Appl. Surf. Sci.*, 2021, **546**, 149019.

53 D. K. Verma, N. Shukla, B. Kumar, A. K. Singh, K. Shahu, M. Yadav, K. Y. Rhee and R. B. Rastogi, *ACS Appl. Mater. Interfaces*, 2019, **11**, 2418–2430.
54 Y. Meng, F. Su and Y. Chen, *Chem. Eng. J.*, 2015, **281**, 11–19.
55 S. Asaldoust, M. S. Hosseini, B. Ramezanzadeh and G. Bahlakeh, *Constr. Build. Mater.*, 2020, **256**, 119439.
56 Y. Wu, X. Zeng, T. Ren, E. D. Vries and V. Emile, *Tribol. Int.*, 2017, **105**, 304–316.
57 I. E. Uflyand, V. A. Zhinzhilo and V. E. Burlakova, *Friction*, 2019, **7**, 93–116.